Jagannath University Journal of Science
Volume 07, Number II, June 2021, pp. 35–46
https://jnu.ac.bd/journal/portal/archives/science.jsp
ISSN 2224-1698

JnUJSci

Numerical Analysis of Steady and Unsteady Fluid Flow and Energy Distribution through a Curved Square Geometry Driven by Variable Pressure Gradients

Research Article

Selim Hussen[1], Ratan Kumar Chanda[1], Tahmina Sultana[2], Rabindra Nath Mondal[1*]

[1]*Department of Mathematics, Jagannath University, Dhaka-1100, Bangladesh*
[2]*Department of Science and Humanities, Military Institute of Science and Technology (MIST), Mirpur Cantonment, Dhaka-1216, Bangladesh.*

Received: 21 January 2021
Accepted: 25 April 2021

Abstract : Because of remarkable applications from medical services to industrial activities, the study of flow and temperature distribution in a coiled geometry has fascinated consideration to the scholars. In the current expedition, a spectral-based numerical innovation is presented for the flow characteristics with energy distribution in a curved square duct (CSD) with lower wall heated and cooling from the ceiling; the two side-walls being thermally insulated. Flow characteristics are governed by the combined action of Grashof number (*Gr*), the curvature (δ) and the Prandtl number (Pr) keeping their values fixed at 1000, 0.1 and 7.0, respectively while the Dean number (*Dn*) is considered a broad range from greater than 0 to 5000. Firstly, we investigate the steady solution (SS) branches and found two branches of SS with 2- to 8-cell solution. Moreover, oscillating behaviors including transitional stages of unsteady flow (UF) is discussed in details. The study shows that the trend of UF changes as *chaotic* to *chaotic* via *steady-state* and *periodic* for progressing value of *Dn*. Flow transition is meticulously measured by attaining phase-portrait of the time-advancement results. Streamlines and isotherms for time-dependent flows show that they consist of asymmetric 2- to 6-cell solution. It is found that the secondary flow influences convective heat transfer (CHT) more effectively and boosts heat transfer substantially with the increase of the secondary vortices that occurs for chaotic oscillations. The correctness of obtaining the current results is confirmed by comparing with existing experimental exposure.

Keywords: *Square-shaped geometry • Streamlines • Isotherm • Phase-space • Heat transfer*

1. Introduction

Two-dimensional (2D) fluid flow behavior through a curved geometry is not only applied in engineering applications such as in chemical reactors, rocket and aircraft engines, heat exchangers, gas turbines, electric generators, air-conditioning, refrigeration, turbo-machinery but also used in biological problems such as in human Lung, blood circulation in vein and arteries. It is noteworthy that there is a basic difference between straight-channel flow and curved-channel flow in terms of creating forces. Curved-shaped duct produces the centrifugal and buoyancy force causing duct curvature and temperature variation respectively. The work of centrifugal body force is mainly on the outer concave wall of the duct. Consequently, the generation of two-vortex secondary flow is transferred into four-vortex under a critical flow condition. The existence of such

*Corresponding author: Rabindra Nath Mondal
E-mail: rnmondal71@yahoo.com

problem was first analyzed by Dean (1927), called the pioneer, who described the flow conditions curiosity. Ever since, several researchers have done many significant studies. The researchers are mentioned to Ligrani and Niver (1988) and Berger *et al*. (1983) for a number of exceptional reviews on curved duct flows.

As bifurcation structure of flow through a curved-geometry influence the fluid flow vortices, so this study has been started from the initial stage of the duct flows. Daskopoulus and Lenhoff (1990) applied finite volume method to investigate bifurcation structure through a circular pipe. For isothermal flow, Mondal *et al*. (2007) disclosed four SS branches with linear stability analysis. Adopting spectral technique, Yamamoto *et al.* (1999) investigated the flow formation and found a 6-cell phenomenon of the swirling flow. Mondal *et al.*(2006) demonstrated the bifurcation for non-isothermal flow by applying spectral method in the curved square channel. Six branches of steady structure where two branches are symmetric and the other branches are asymmetric have been described by Wang *et al*. (2005) where they have implemented the Euler-Newton continuation technique with the bifurcation testing function. A detailed pore-scale study by spectral-based method for counter and co-rotating of the curved square duct is available in literature by Mondal *et al*. (2014) who studied solution structure, stability and transitions of the flow in detail.

The understanding of the unsteady flow behaviors is of fundamental importance. Wang *et al*. (2005) studied numerically and experimentally the periodic fluctuations for an incompressible fluid in a curved square duct (CSD) and the comparison shows excellent agreement between both the results. Chandratilleke and Nursubyakto (2003) performed numerical approach to elucidate the flow properties through the variable geometries of different aspect ratios with warm the outer wall. Mondal *et al*. (2013) conducted numerical method to analyze the flow transition in a curved channel (CC). They investigated the impacts of *Dn* and *Gr* number on the secondary flow pattern. Islam *et al*. (2017) deliberated the influence of *Dn*'s over a wide range of *Tr* on transition in rotating curved channel flows. However, most of the relevant studies only focused on the weak rotational speed, while the transient solution with coupled impacts on buoyancy-influenced centrifugal-Coriolis unsteadiness in a rotating curved rectangular channel (CRC) for highly gyratory speed are not considered though it has numerous engineering applications such as in plastic and metallic industry, cooling systems and cement industry. Hence, motivated from these unresolved issues, the present study deals with the effects of Dean number on unsteady fluid flow in a curved square-shaped duct of moderate curvature.

To progress the conception of thermo-fluid behavior and CHT in a CD, Chandratilleke and Nursubyakto (2003) disclosed that CHT at the concave edge of the curved duct is more capable than that in a SD and the contribution of Dean vortices is to promote temperature distribution (TD) in CC. Yanase *et al*. (2002) and Mondal *et al*. (2014) performed mathematical simulation to examine the fluctuation of flow performance in a curved geometry and recognized that secondary flows (SFs) boost TD. Hasan *et al*. (2019a, 2019b) conducted numerical approach of fluid flow and HT in a rotating curved square-shaped channel (CSC) for various curving. They performed positive rotating case and investigated united impacts of the centrifugal, Coriolis and buoyancy forces. They showed time-progression flow experiences via different flow unsteadiness. Very recently, Roy *et al*. (2020) applied spectral method to predict hydrodynamic instability and CHT through a rotating CRC of moderate curvature. However, the transitional nature of time-dependent flow is still unresolved for the flow having square-shaped geometry with temperature variation between top and bottom walls with changing pressure gradients, which inspired us to fill up this gap.

In this study, the development of the complex flow behavior in the thermal flow transition in a square channel with stream-wise curvature while identifying the influence from the various flow and geometrical parameters is investigated for various Dean numbers. The main objective of this study is, therefore, to investigate the flow characteristics and energy distribution by spectral-based numerical simulation for flow through a curved square-shaped geometry whose bottom wall is heated while cooling from the ceiling. Flow structure as well as transient flow behavior with convective heat transfer is also investigated in detail.

2. Flow Geometry and Mathematical Formulation

Consideration is given for fully developed 2D flow which passes a CSD. Figure 1 illustrates the cross-sectional view and the coordinate system of the computational domain with necessary notations. The bottom and top walls of the working system are considered to be heated and cooled respectively; the upright walls are well insulated to prevent any heat loss. The fluid passes through consistently in the stream-wise direction as exhibited in Figure 1.

The stream functions for cross-sectional velocities have the following form

$$u = \frac{1}{r}\frac{\partial \psi}{\partial y} \quad \text{and} \quad v = -\frac{1}{r}\frac{\partial \psi}{\partial x} \tag{1}$$

where $r = 1 + \delta x$.

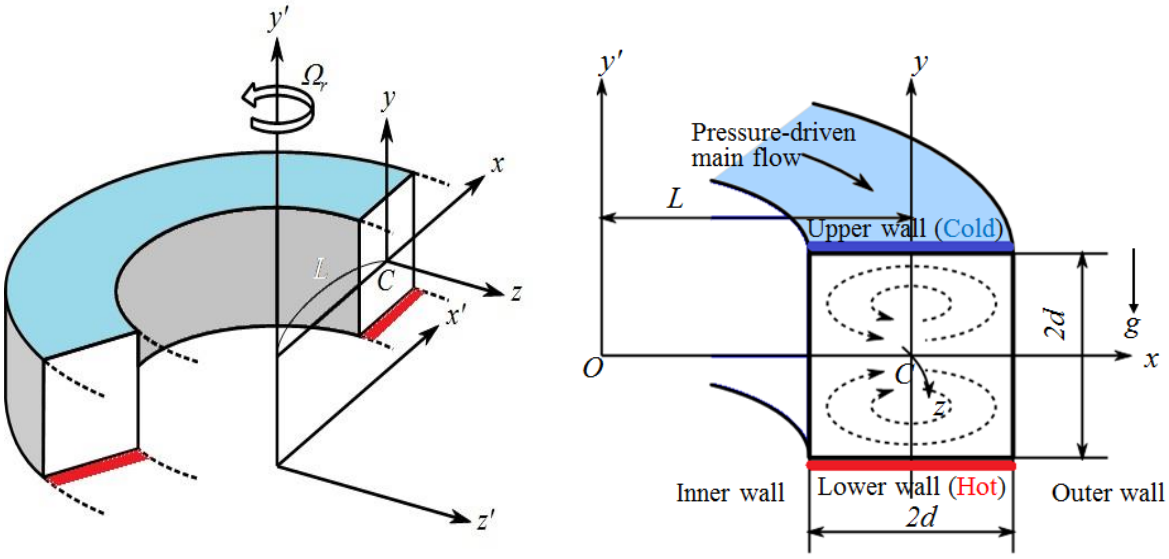

Figure 1. (a) Physical model and coordinate system; (b) Cross-sectional view

Then, non-dimensionalized basic equations for ω, η and ξ are as follows

$$r\frac{\partial\omega}{\partial t}=Dn+r\Delta_2\omega-\frac{\partial(\omega,\eta)}{\partial(x,y)}-\frac{\delta^2\omega}{r}-\frac{\delta}{r}\frac{\partial\eta}{\partial y}\omega+\delta\frac{\partial\omega}{\partial x} \quad (2)$$

$$\left(\Delta_2-\frac{\delta}{r}\frac{\partial}{\partial x}\right)\frac{\partial\eta}{\partial t}=-\frac{1}{r}\frac{\partial(\Delta_2\eta,\eta)}{\partial(x,y)}+\frac{\delta}{r^2}\left[\frac{\partial\eta}{\partial y}\left(2\Delta_2\eta\right)-\frac{3\delta}{r}\frac{\partial\eta}{\partial x}+\frac{\partial^2\eta}{\partial x^2}\frac{\partial\eta}{\partial x}\frac{\partial^2\eta}{\partial x\partial y}\right]$$
$$+\frac{\delta}{r^2}\times\left[3\delta\frac{\partial^2\eta}{\partial x^2}-\frac{3\delta^2}{r}\frac{\partial\eta}{\partial x}\right]-\frac{2\delta}{r}\frac{\partial}{\partial x}\Delta_2\eta+\omega\frac{\partial\omega}{\partial y}$$
$$+\Delta_2{}^2\eta-Gr\times r\frac{\partial\xi}{\partial x} \quad (3)$$

and, $$\frac{\partial\xi}{\partial t}=\frac{1}{\mathrm{Pr}}\left(\Delta_2\xi+\frac{\delta}{r}\frac{\partial\xi}{\partial x}\right)-\frac{1}{r}\frac{\partial(\xi,\eta)}{\partial(x,y)} \quad (4)$$

The dimensionless parameters, the Dean number Dn; the Grashof number Gr and the Prandtl number Pr are defined as:

$$Dn=\frac{Gd^3}{\mu\upsilon}\sqrt{\frac{2d}{L}},\ Gr=\frac{\beta g\Delta Td^3}{\upsilon^2},\mathrm{Pr}=\frac{\upsilon}{\kappa} \quad (5)$$

Along with boundary condition for ω and η as

$$\left.\begin{aligned}\omega=\eta=\frac{\partial\eta}{\partial x}=0, x=\pm1, y=y\\ \omega=\eta=\frac{\partial\eta}{\partial y}=0, x=x, y=\pm1\end{aligned}\right\} \quad (6)$$

Boundary condition for temperature ξ is

$$\xi(x,1)=1,\xi(x,-1)=-1,\xi(\pm1,y)=-y \quad (7)$$

3. Numerical simulation

3.1 Method of numerical procedure

For finding the numerical solution from equations (2) to (4), spectral technique along with the expansion by polynomial functions and Chebyshev polynomials is applied at the obtained dimensionless momentum and energy equations. That is, the functions expansion of $\phi_n(x)$ and $\eta_n(x)$ are articulated as

$$\left.\begin{aligned}\phi_n(x)=(1-x^2)C_n(x),\\ \eta_n(x)=(1-x^2)^2C_n(x)\end{aligned}\right\} \quad (8)$$

where, $C_n(x)=\cos\left(n\cos^{-1}(x)\right)$ is the n^{th} order Chebyshev polynomial. $\omega(x,y,t)$, $\eta(x,y,t)$ and $\xi(x,y,t)$ are expanded in terms of $\phi_n(x)$ and $\eta_n(x)$ as

$$\left.\begin{aligned}\omega(x,y,t)=\sum_{m=0}^{M}\sum_{n=0}^{N}\omega_{mn}(t)\phi_m(x)\phi_n(y),\\ \eta(x,y,t)=\sum_{m=0}^{M}\sum_{n=0}^{N}\eta_{mn}(t)\eta_m(x)\eta_n(y),\\ \xi(x,y,t)=\sum_{m=0}^{M}\sum_{n=0}^{N}\xi_{mn}(t)\phi_m(x)\phi_n(y)-y.\end{aligned}\right\} \quad (9)$$

where M and N represent the truncation numbers in the x- and y- directions respectively, and ω_{mn}, η_{mn} and ξ_{mn} are the coefficients of expansion. The collocation points (x_i, y_j) are taken to be

$$x_p = \cos\left[\pi\left(1-\frac{p}{M+2}\right)\right],\ y_q = \cos\left[\pi\left(1-\frac{q}{N+2}\right)\right]. \quad (10)$$

To achieve steady solutions $\bar{\omega}(x,y)$, $\bar{\eta}(x,y)$ and $\bar{\xi}(x,y)$, the expansion series (9) with coefficients $\omega_{mn}(t)$, $\eta_{mn}(t)$ and $\xi_{mn}(t)$ are converted into the basic equations (2) - (4), abide by applying the collocation method. To obtain unsteady solutions, the Crank-Nicolson and Adams-Bashforth methods composed with the function expansion (9) and the collocation methods are applied to Eqs. (2) to (4). The processes included in the methods are detailed in Mondal (2007).

3.2 Hydraulic resistance coefficient

The hydraulic resistance coefficient λ is defined as

$$\frac{\bar{p}_1-\bar{p}_2}{\Delta_{\bar{z}}} = \frac{\lambda}{\bar{d}_h}\frac{1}{2}\rho\langle\bar{\sigma}\rangle^2 \quad (11)$$

where $\bar{d}_h$ is the hydraulic diameter. The mean axial velocity $\langle\bar{\sigma}\rangle$ is calculated by

$$\langle\bar{\sigma}\rangle = \frac{\nu}{4\sqrt{2\delta d}}\int_{-1}^{1}dx\int_{-1}^{1}\sigma(x,y,t)\,dy \quad (12)$$

λ is related to the mean non-dimensional axial velocity $\langle\sigma\rangle$ as

$$\lambda = \frac{4\sqrt{2\delta}Dn}{\langle\sigma\rangle^2} \quad (13)$$

Using the mathematical approach, the value of λ can be calculated from equation (13).

4. Results and Discussion

In the ongoing investigation, the characteristics of incompressible fluid flow through a CSD under the impact of rotation and applied temperature difference has been accomplished. In addition, curvature $\delta = 0.1$, Prandtl number Pr = 7.0 and Dean number $Dn\,(0 < Dn \le 5000)$ are also considered.

4.1 Combined branching structure

A comprehensive investigation of the combined branching structure of the SS branch is performed and thereafter discuss the obtained branches individually. Numerical technique path continuation method is employed to achieve more sensible results. We obtain two branches of SS which are distinguished by different colors and line patterns for $0 < Dn \le 5000$ and Gr = 1000. Figures 2(a) and 2(b) are presented for combined branching structure and magnification of Fig. 2(a) respectively. The two SS branches are named *branch* 1 (first branch) and *branch* 2 (second branch). The special remark here is that no bifurcating connectivity between the two branches of steady solutions is observed.

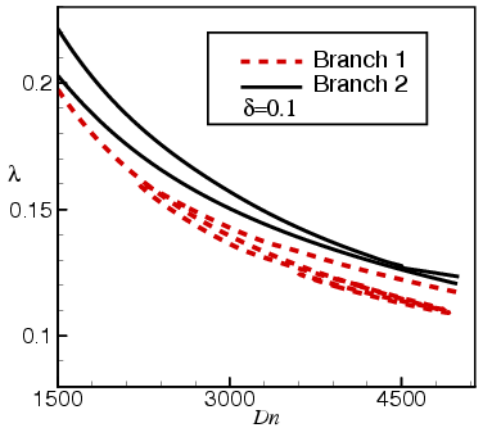

(a)

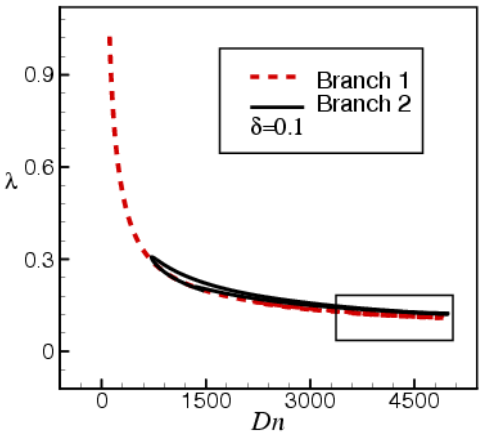

(b)

Fig. 2. (a) Branching structure for $0 < Dn \le 5000$
(b) Magnification of Fig. 2(a) at larger Dn

First branch

Firstly, between the two branches, the first branch has been plotted exclusively in Fig. 3(a) and for more clear visualization, enlargements of the Fig. 3(a) at larger *Dn* have been shown in Figs. 3(b) and 3(c) for $0 < Dn \le 5000$. Between the two branches of SS, this branch possesses the whole region of *Dn*. The branch 1 is entangled with four turnings in the whole branch which are marked in the positions *b, c, d*. The trend from point *a* to point *e* goes in the sequence $a(Dn \approx 100) \rightarrow d(Dn \approx 4800) \rightarrow c(Dn \approx 3699) \rightarrow (Dn \approx 4902) \rightarrow b(Dn \approx 2299) \rightarrow e(Dn \approx 5000)$.

The turning points are smooth (see Figs. 3(b) and 3(c)). Figure 4 represents the pattern of secondary flows (SF) and isotherm for several *Dn*. It is clear that the number of Dean vortex increases for increasing the Dean number. The reason is that a centrifugal forces had been formed as the bottom wall heated and the cooling from the ceiling of our curved geometry. The flows were noted to be symmetric multi-vortex solution. The investigated results have been shown in Figure 4 at different turning points of the siolution curve as shown explicitly in Figure 3.

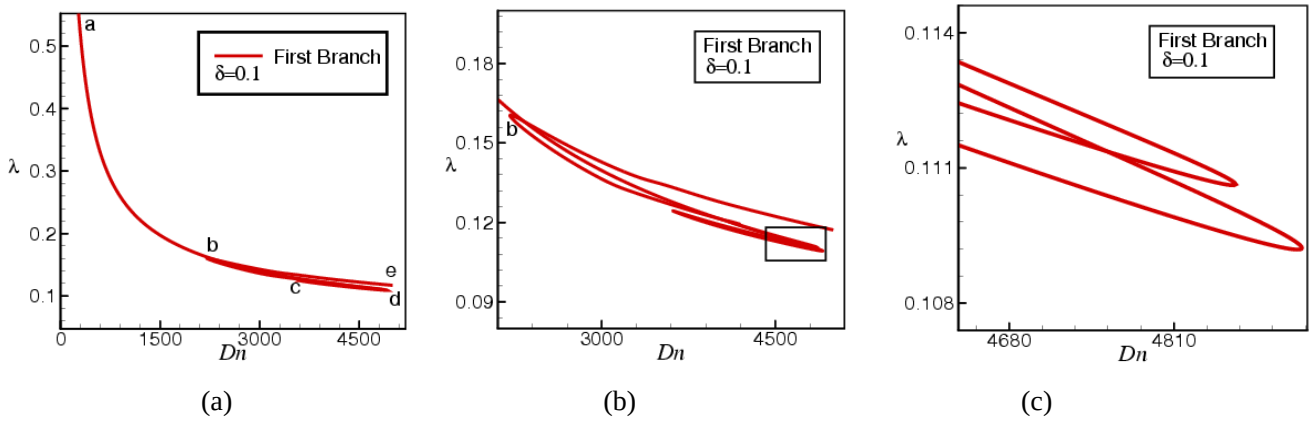

(a) (b) (c)

Figure 3.(a) First branch (b) Magnification of Fig. 3(a) about point d and (c) Magnification of Fig. 3(b) at large *Dn*.

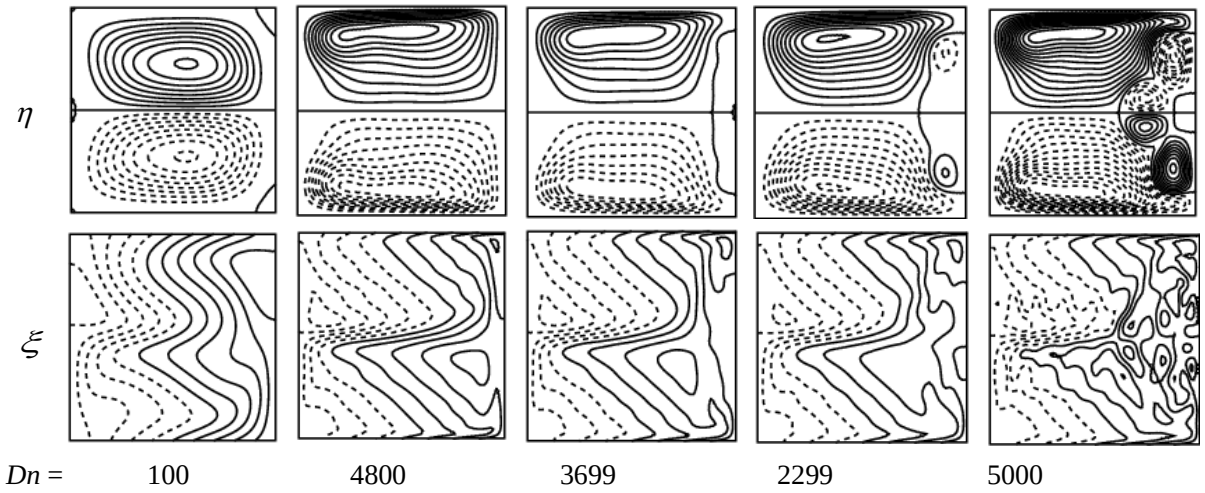

Figure 4. Pattern variation of SF and isotherms on the first branch for different *Dn* at $\delta = 0.1$

Second branch

The second branch of SS is presented in Fig. 5(a). Figure 5(b) represents the magnification of Fig. 5(a). From these figures, we see that this branch has three smooth turning points as shown by *b, c, d*. The branch starts at point $a\,(Dn = 5000)$ and it goes at the point $d\,(Dn = 796)$ with two turnings say $b\,(Dn = 1398)$ and $c\,(Dn = 1473)$ then turns in the opposite direction and finally reaches at point $e(Dn = 5000)$. Figure 6 exhibits the pattern of SF and isotherm and it is stating that the branch consists of 4-vortex solution. It is identified that the streamlines of

the Dean flow are comprised with two or more counter rotating large-sized primary vortices which called efferent and intimate flow in the direction of anti-clockwise and clock-wise indicated by thick solid and dotted lines respectively. The fluid is accelerated by the combined action of the centrifugal force, caused due to curvature of the duct, and the buoyancy force due to temperature difference between the two walls. The flow becomes asymmetric due to these combined forces. Figure 6 explicitly shows pattern variation of secondary flows and isotherms on the second branch for different values of *Dn* at $\delta = 0.1$

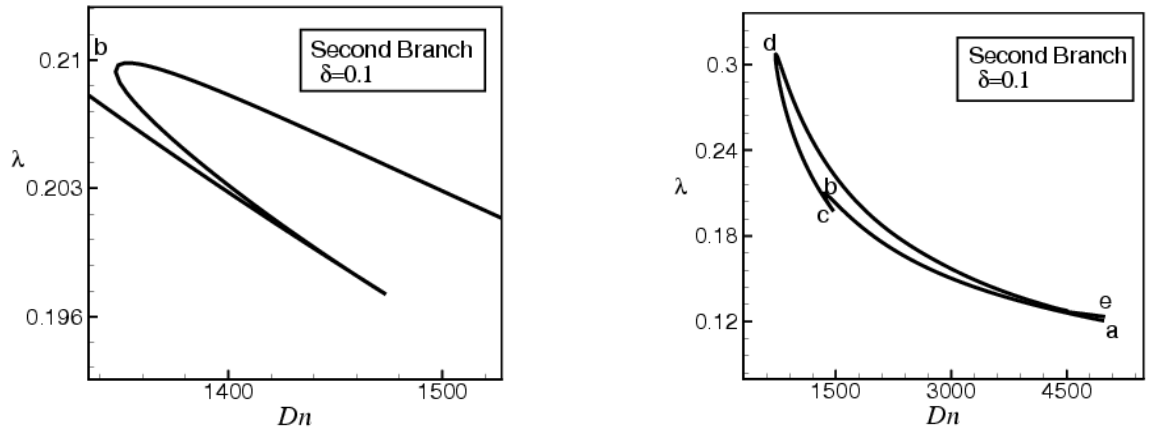

Figure 5. (a) Second steady branch (b) Magnification of Fig. 5(a) about point *b*.

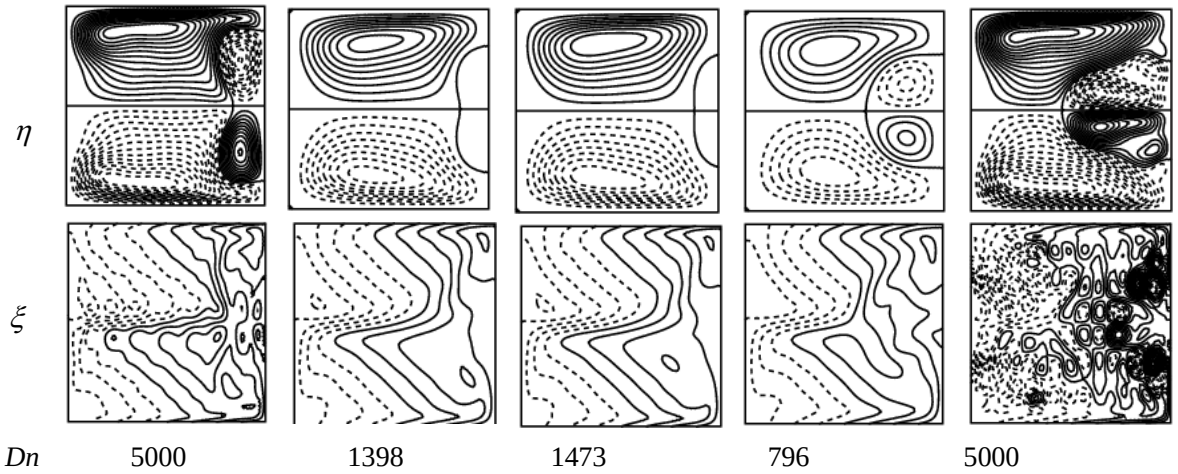

Figure 6. Pattern variation of SF and isotherms on the second branch for different *Dn* at $\delta = 0.1$

4.2 Time-dependent solution

For analyzing the oscillating behavior with the values of λ for SS for the mentioned *Dn* at $\delta = 0.1$ pointed out by straight lines which use the same sort of lines as used in Figure 2(a).The flow state is also justified by graphing phase space (PS). We calculate the oscillating behavior for *Dn* = 10, *Dn* = 40, *Dn* = 80. It is clear observation that the flow is periodic for *Dn* = 10 and *Dn* = 40 and the time-progression result is found that a chaotic solution with asymmetric 3-vortex solution for *Dn* = 80 as depicted in Figs. 7(a) and 7(c). For clear observation of chaotic nature, we plot phase space diagram as shown in Fig. 7(b). It is worth mentioning that the orbits intersect each other which confirm the chaotic solution. In addition, the flow moves around $\lambda = 1.13$ and fluctuates below the SS which means the transitional chaos. Again, we performed the oscillating behavior of λ for $Dn = 500$, $Dn = 1000$, $Dn = 2500$ and it is worth mentioning that the flow is steady-state with asymmetric two vortex solution for each three cases as depicted in Figs. 8(a) and 8(b); Figs. 9(a) and 9(b); and in Figs. 10(a) and 10(b), respectively.

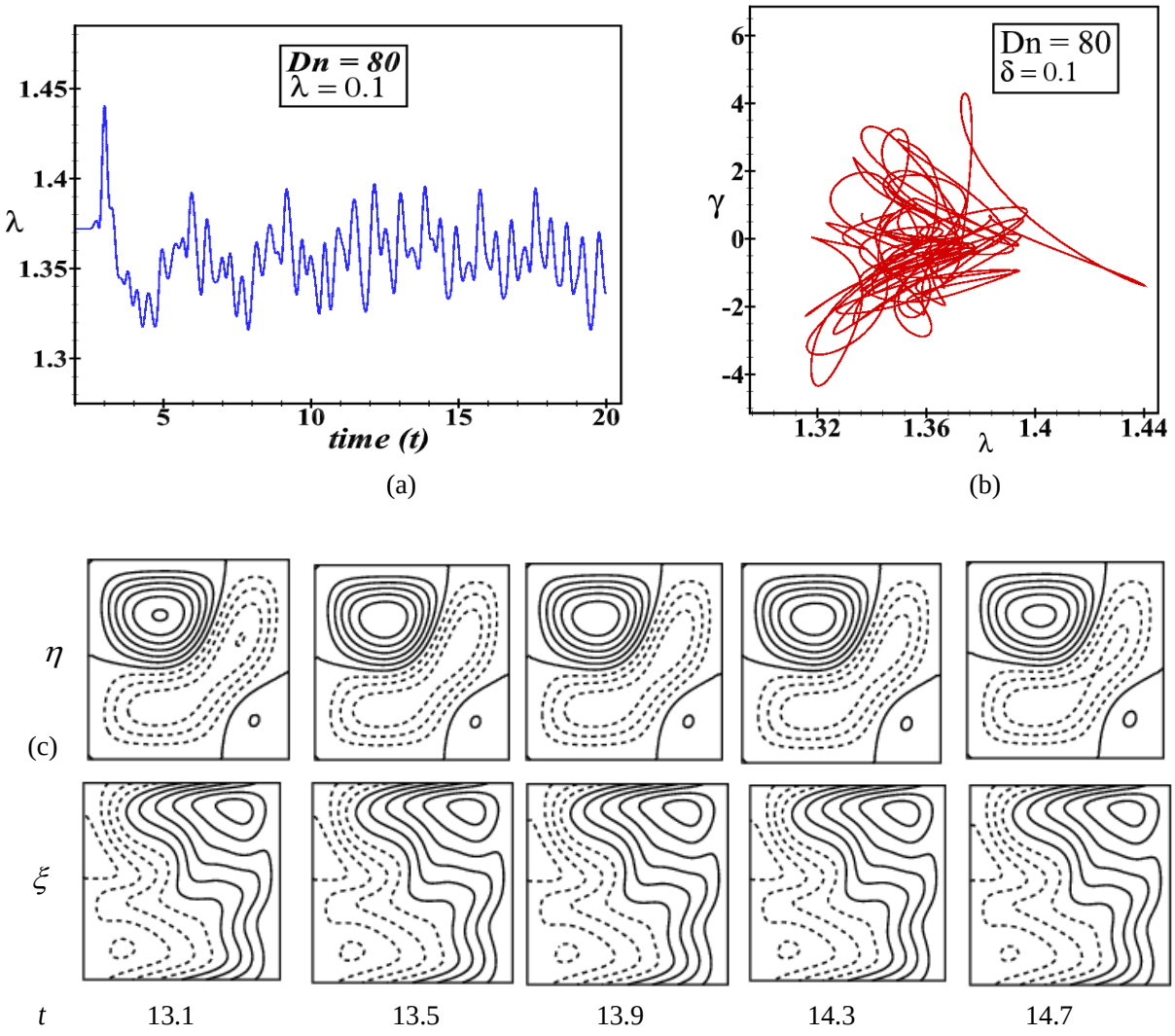

Figure 7. (a) Time-advancement for $Dn = 80$ (b) Phase-space for $Dn = 80$ (c) Pattern variation of SF and isotherms for $13.1 \le t \le 14.7$.

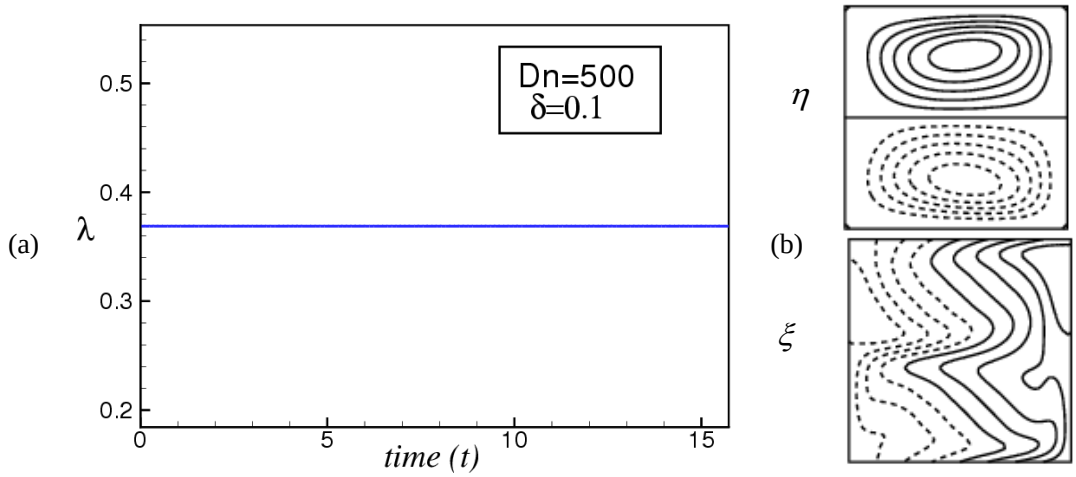

Figure 8. (a) Time-advancement for $Dn = 500$ (b) Pattern variation of SF and isotherm at $t = 10.4$.

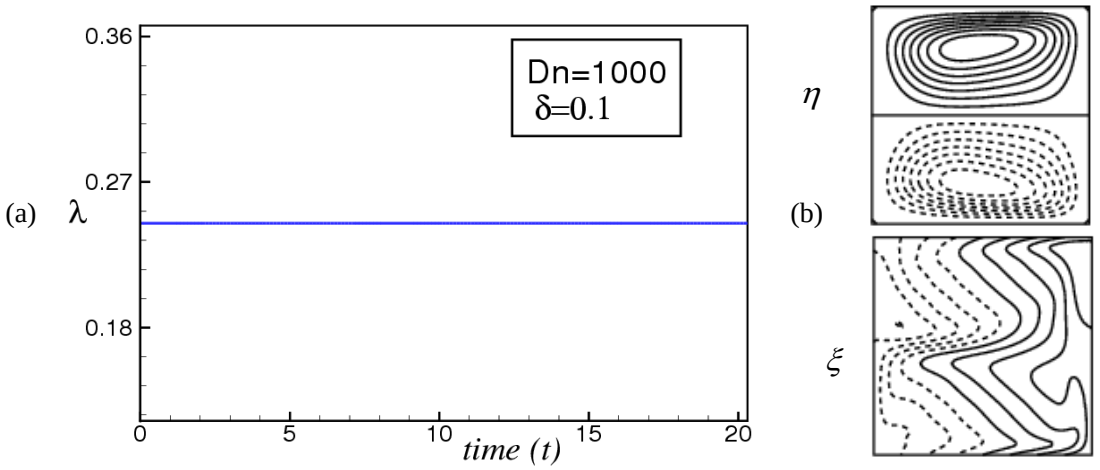

Figure 9. (a) Time-advancement of λ for $Dn = 1000$ (b) Pattern variation of SF and isotherm at $t = 20$.

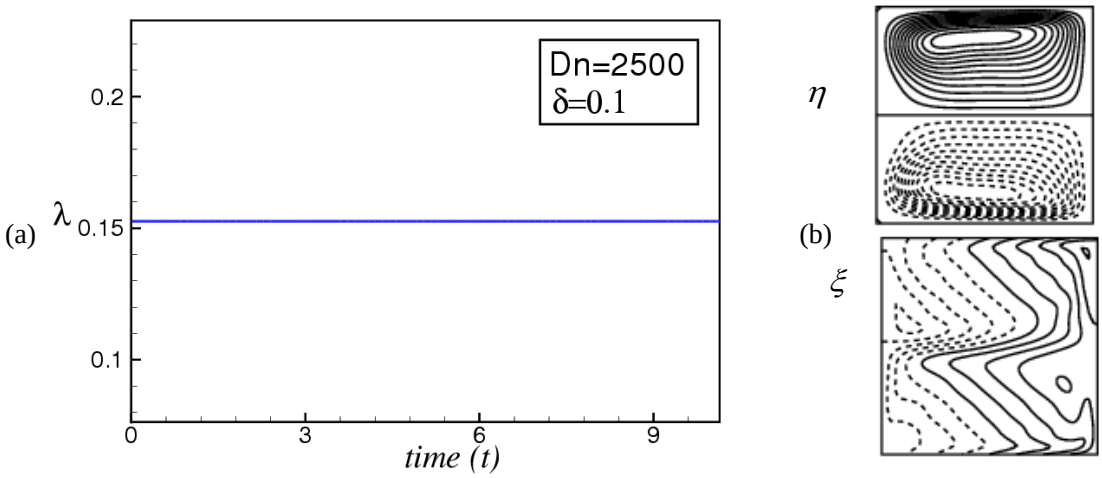

Figure 10. (a) Time-advancement of λ for $Dn = 2500$. (b) Pattern variation of SF and isotherm at $t = 8.0$.

As Dn is increased gradually, and at Dn = 3500, the steady-state flow transforms into periodic with 2-vortex solution (Figs. 11(a) and 11(c)).To be confirm whether the flow is periodic or not we draw PS diagram as elucidated in Fig. 11(b). It can be seen that the orbits do not intersect each other which validates the periodic flow. The time-advancement procedure had been continued over and over again for $Dn = 4000$, the flow fluctuates haphazardly that means the flow is chaotic with 2- to 4-vortex solution as evidences in Figs. 12(a) and 12(c), respectively. Figure 12(b) represents phase portrait which gives proof of the chaotic oscillation. Furthermore, the flow moves around $\lambda = 0.127$ and the same flow nature continues to $Dn = 5000$ as illustrated in Figs. 13(a), 13(b) and 13(c). It is observed that mostly fluid velocity that get generated neighboring the concave wall and energy distributions are expressively circulated that makes more heat energy which moved to fluid from the concave wall. Note that, Mondal *et al*. (2006) conducted numerical simulation of viscous incompressible flow and heat transfer through a rotating curved square-shaped channel with constant curvature and identified transitional behavior of the flow with vortex structure of secondary flows. Next, Mondal *et al*. (2015) applied spectral-based numerical approach to evaluate non-isothermal flow characteristics in a curved square-shaped duct in a rotating system and reported flow transition in details.

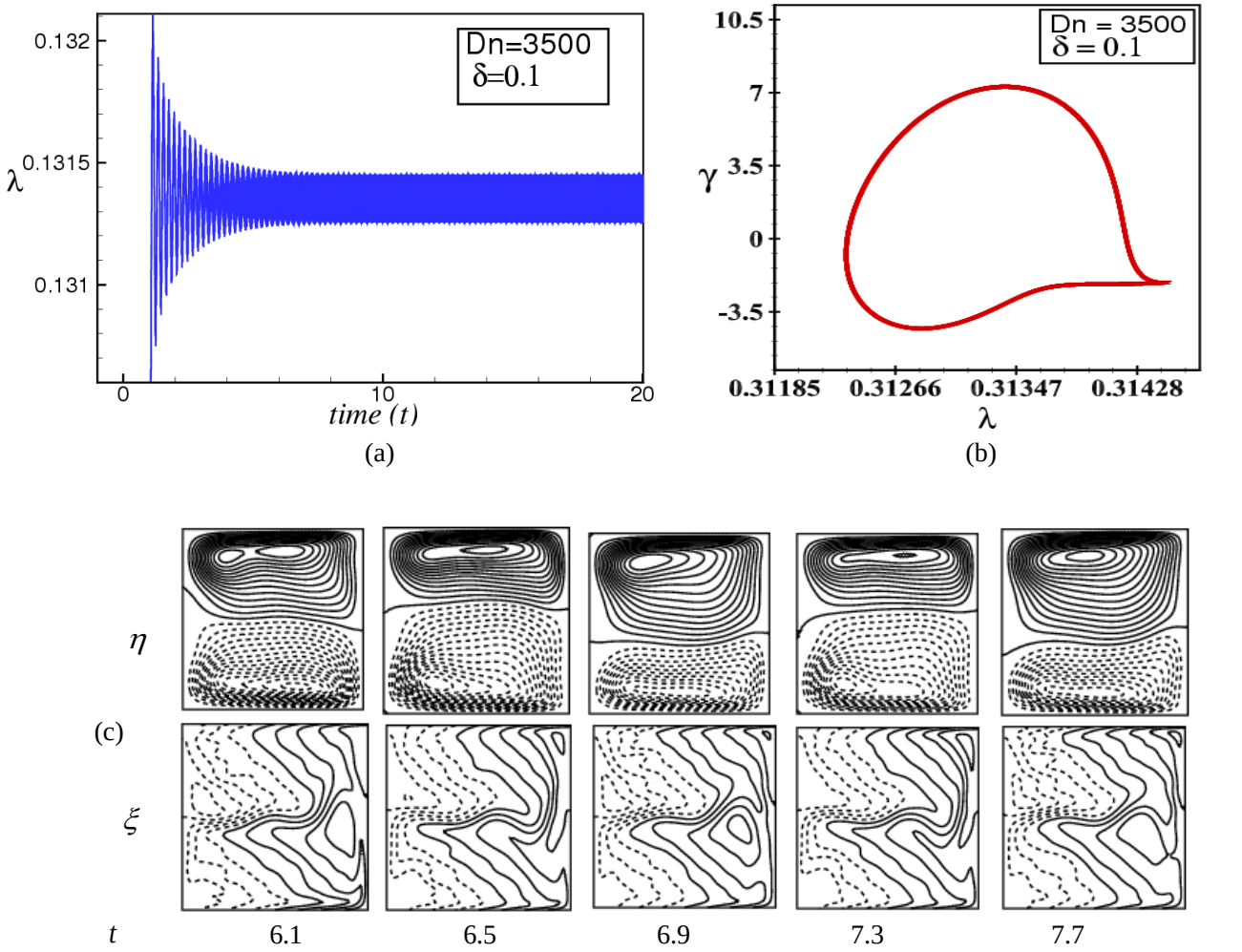

Figure 11. (a) Time-advancement of λ for *Dn* = 3500 . (b) Phase-space for *Dn* = 3500 (c) Pattern variation of SF and isotherms for $6.1 \le t \le 7.7$

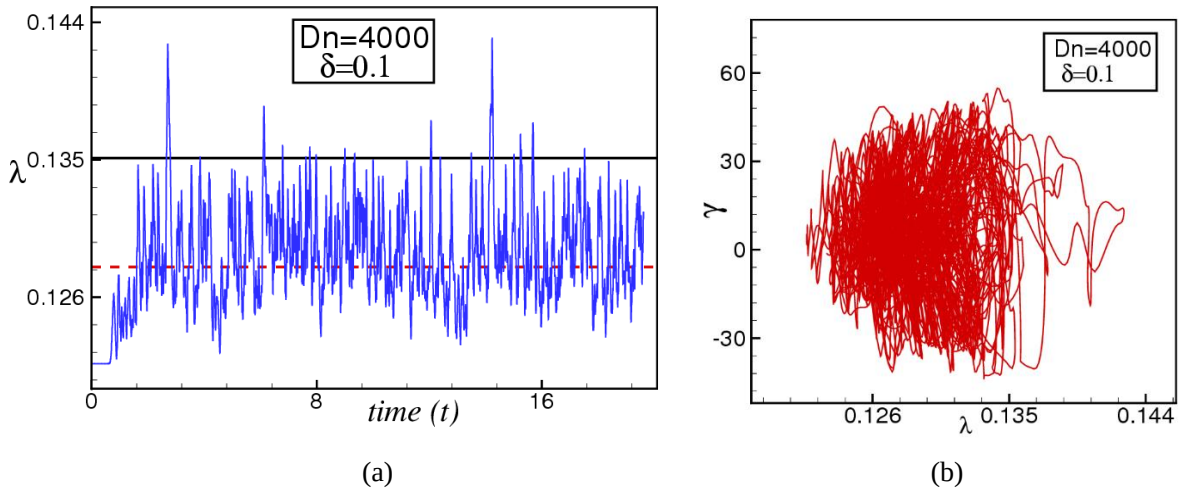

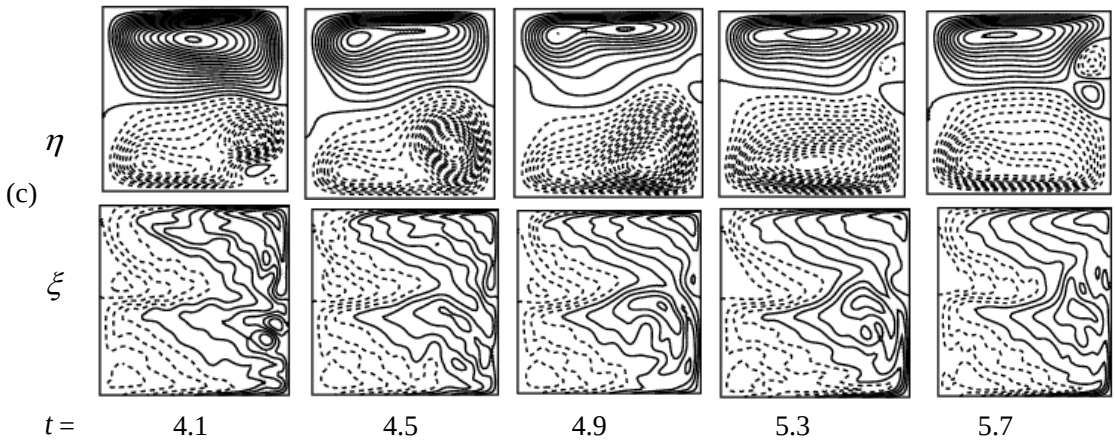

Figure 12. (a) Time-advancement of λ for $Dn = 4000$. (b) Phase-space for $Dn = 4000$ (c) Pattern variation of SF and isotherms for $4.1 \le t \le 5.7$.

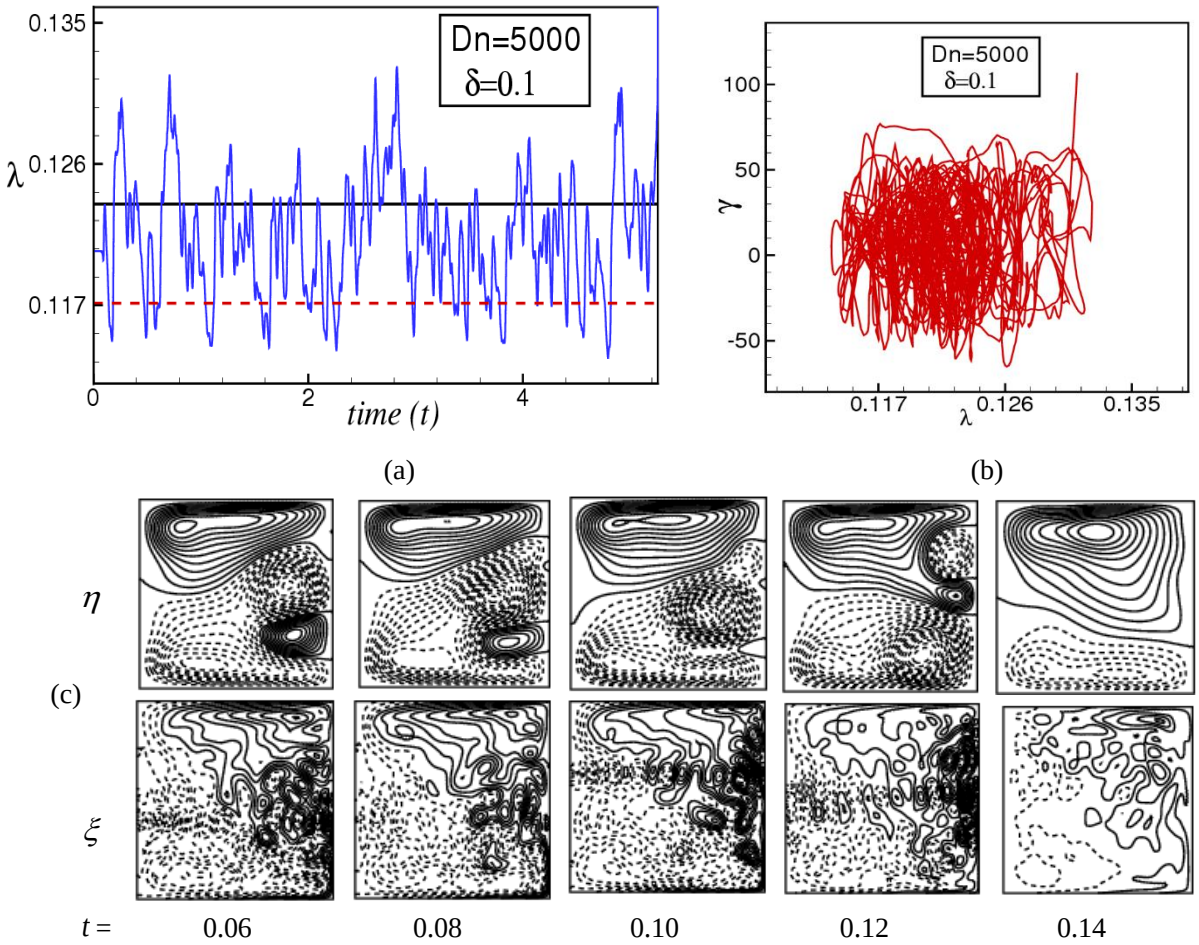

Figure 13. (a) Time-advancement of λ for $Dn = 5000$. (b) Phase-space for $Dn = 5000$ (c) Pattern variation of SF and isotherms for $0.06 \le t \le 0.14$.

4.3 Convective Heat Transfer

To discuss convective heat transfer (CHT) from the hot wall to the fluid, the temperature gradient (TG) for both horizontal wall has been executed. Figures 14(a) & 14(b) display the corresponding TG for cool and hot wall respectively. It can be noted that the TG for cool wall decreases and possesses the tendency to become zero in the middle region around *x*-axis as *Dn* increases except at *Dn* = 500. The centrifugal force and corresponding

convective heat generation to the outward direction influence the HT at the center of the wall. On the contrary, the TG for hot edge increases in the middle region as *Dn* increases except for *Dn* = 500 and *Dn* = 1000 and it increases monotonically for larger *Dn*.

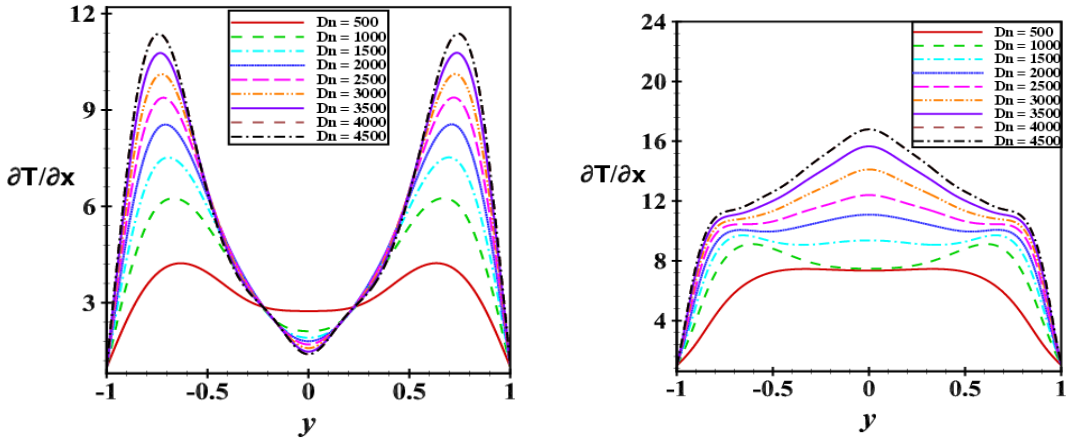

(a) (b)

Figure 14. (a) TG at the cooling wall (b) TG at the heated wall

4.4 Validation

The validation of obtaining numerical results is confirmed by comparing the results of existing experimental data in literature. Figures 15(a) and 15(b) present a relative comparison of our numerical findings with the experimental investigations obtained by Bara *et al*. (1992) and Mees *et al*. (1996) for a CSD flow. Figure on the left of each pair is the secondary flow pattern for experimental outcomes and right figure shows our numerical result. As seen in Figure 15, our numerical approach has a good match with the experimental measurements, which justifies the accuracy of the present numerical study.

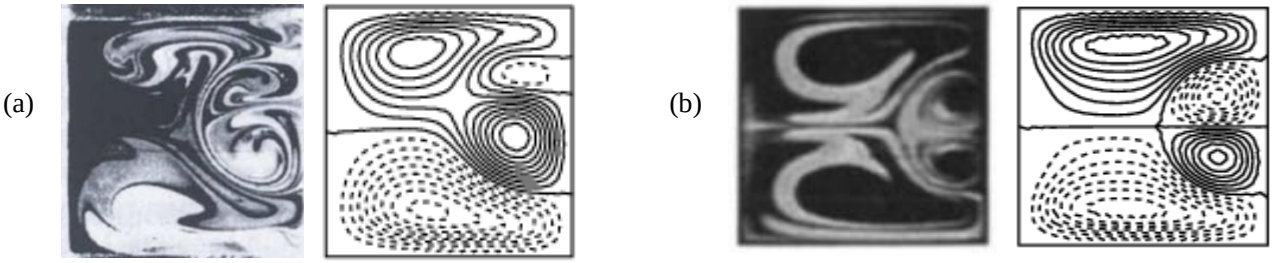

(a) *Dn* =200 $\left(\theta = 90^{\circ}\right)$ *Dn* =209 (b) *Dn* =150$\left(\theta = 240^{\circ}\right)$ *Dn* =176

Figure 15. Comparison of numerical data with experimental outcomes. Left: Experimental result by (a) Bara *et al*. (1992), (b) Mees *et al*. (1996) and right: numerical result by the authors.

5. Concluding remarks

The present study is a spectral-based numerical innovation for flow characteristics and energy distribution in a curved square-shaped duct with lower wall heated and cooling from the ceiling; the two side-walls being thermally insulated. We considered various parameters for controlling the flows like the Grashof number, curvature, the Prandtl number and the Dean number (*Dn*). The following conclusions have been drawn from the present study;

- An asymmetric two branches of SS are obtained comprising with 2- to 8-vortex solutions on various branches.
- Time-progression as well as PS analysis demonstrates that transient flow develops in the sequence of "*chaotic* $\rightarrow$ *steady-state* $\rightarrow$ *periodic* $\rightarrow$ *chaotic*", for increasing *Dn*.
- Velocity contours show that there exist axisymmetric 2-vortex solution for the steady-state, and 2- to 4-vortex for the periodic and chaotic oscillation respectively.
- Convective heat transfer is increased with the increase of rotation. The highly complex secondary flow filed is developed with higher *Dn*, and HT is boosted substantially by the chaotic solutions than the other flow state.

- The current study shows that there arises a strong interaction between the heating-induced buoyancy force and the centrifugal instability in the curved channel that stimulates fluid mixing and thereby increases heat transfer in the fluid**.**

References

Bara B, Nandakumar K, Masliyah JH. (1992). An experimental and Numerical study of the Dean Problem: flow development towards two-dimensional multiple solutions, *J. Fluid Mech*., 244: 339-76.

Berger SA, Talbot L, Yao LS. (1983). Flow in Curved Pipes, *Annual. Rev. Fluid. Mech*., 35: 461-512.

Chandratilleke TT and Nursubyakto K. (2003). Numerical prediction of secondary flow and convective heat transfer in externally heated curved rectangular ducts, *Int. J. Thermal Sciences*, 42: 187-198.

Daskopoulos P and Lenhoff AM (1990). Flow in curved ducts, Part 2, Rotating ducts, *Journal of Fluid Mechanics*, 217: 575-93.

Dean WR. (1927). Note on the motion of fluid in a curved pipe, *Philos Mag*. 4: 208-223.

Hasan MS., Mondal RN. and Lorenzini G. (2019b). Numerical Prediction of Non-isothermal Flow with Convective Heat Transfer through a Rotating Curved Square Channel with Bottom Wall Heating and Cooling from the Ceiling, *Int. J. Heat and Technology*, 37(3): 710-720.

Hasan M S, Mondal R N. And Lorenzini G. (2019b).Centrifugal Instability with Convective Heat Transfer through a Tightly Coiled Square Duct, *Mathematical Modelling of Engineering Problems*, 6(3): 397-408.

Islam MZ, Mondal RN, Rashidi MM. (2017). Dean-Taylor flow with convective heat transfer through a coiled duct, *Computers and Fluids*, 149: 41-55.

Ligrani, PM, and Niver RD. (1988). Flow Visualization of Dean Vortices in a Curved Channel with 40 to 1 Aspect Ratio, *Physics of Fluids*, 31(12): 3605.

Mees PAJ, Nandakumar K, Masliyah JH.(1996). Secondary Instability of Flow in a Curved Duct of Square Cross Section, *Journal of Fluid Mechanics*, 323: 387-409.

Mondal RN, Kaga Y, Hyakutake T and Yanase S. (2006). Effects of curvature and convective heat transfer in curved square duct flows, *Trans. ASME, Journal of Fluids Engineering*, 128(9): 1013-1022.

Mondal RN, Kaga Y, Hyakutake T and Yanase S (2007). Bifurcation Diagram for Two-dimensional Steady Flow and Unsteady Solutions in a Curved Square Duct, *Fluid Dynamics Research*, 39: 413-446.

Mondal, RN, Islam, MZ, Islam, MM and Yanase, S. (2015). Numerical prediction of non-isothermal flow through a rotating curved duct with square cross-section, *Thammasat Int. J. Sci. Tech.*, 20(4): 1 -20.

Mondal RN, Ray SC and Islam S. (2014a). Solution structure, stability and pattern variation of secondary flows through a rotating curved duct with rectangular cross section, *International Journal of Energy & Technology*, 6(5): 1-12.

Mondal RN, Islam MS, Uddin K. and Hossain MA. (2013). Effects of aspect ratio on unsteady solutions through curved duct flow, *Applied Mathematics and Mechanics*, 34(9): 1107–1122.

Mondal RN, Ray SC and Yanase S. (2014b).Combined Effects of Centrifugal and Coriolis Instability of the Flow through a Rotating Curved Duct with Rectangular Cross Section.*Open Journal of Fluid Dynamics*, 4: 1-14.

Razavi SE, Soltanipour H., Choupani P. (2015). Second law analysis of laminar forced convection in a rotating curved duct. *Thermal Sciences*, 19(1): 95-107.

Roy SC, Hasan MS and Mondal RN. (2020). On the Onset of Hydrodynamic Instability with Convective Heat Transfer through a Rotating Curved Rectangular Duct, *Mathematical Modelling of Engineering Problems*, 7(1): 31-44.

Selmi M., Nandakumar K. and Finlay WH. (1994).A bifurcation study of viscous flow through a rotating curved duct, *J. Fluid Mechanics*, 262: 353-375.

Wang L, Pang O and Cheng L (2005). Bifurcation and stability of forced convection in tightly coiled ducts: multiplicity, *Chaos, Solitons and Fractals*, 26: 337-352.

Wang L. and Yang T. (2005). Periodic oscillation in curved duct flows, *Physica D*, 200: 296-302.

Yamamoto K, Yanase S. and Alam MM. (1999). Flow through a rotating curved duct with Square Cross-section, *J. Phys. Soc. Japan*, 68: 1173-1184.

Yanase S, Kaga Y. and Daikai R. (2002). Laminar flow through a curved rectangular duct over a wide range of the aspect ratio, *Fluid Dynamics Research*, 31: 151-183.